NUCLEAR THEORY, Vol. 36 (2017)
eds. M. Gaidarov, N. Minkov, Heron Press, Sofia

On Decays of Atomic Nuclei by Emission of Clusters, Light Particles and Fission

K. Pomorski[1], **B. Nerlo-Pomorska**[1], **M. Warda**[1], **A. Zdeb**[1], **J. Bartel**[2], **C. Schmitt**[2]

[1]UMCS, 20031 Lublin, Poland
[2]IPHC, 67000 Strasbourg, France

Abstract. A simple WKB model, able to describe the emission of protons, α-particles and nuclear clusters as well as the spontaneous fission process, is presented. Potential energy surfaces of fissioning nuclei are determined within the macroscopic-microscopic model, using a new Fourier-type shape parametrisation and fission-fragment mass distributions are calculated.

1 Introduction

A very large majority of today known nuclei are radioactive and decay by β radioactivity, by the emission of protons, α particles and heavier clusters or by spontaneous fission. Their half-lives are determined by calculating the penetrability of the charged particle or the entire nucleus through the potential-energy barrier from the inside. Section 2 presents an approach, similar to the Gamow model [1], for the emission of protons, α particles and clusters. The results for the barrier penetrability are adjusted with a single parameter for even-even nuclei (plus one additional common for odd A and odd-odd nuclei) and compared to other models. Section 3 explains how we estimate in a simple way the spontaneous-fission probability. This analysis is carried out using a new Fourier shape parametrisation given in detail in Section 4. Some examples of potential-energy surfaces as functions of several deformation parameters are presented in Section 5, before giving conclusions and perspectives.

2 A Gamow-Like Model for the Decay of Charged Particles

Half-lives of nuclei with respect to the decay by light-particle emission can be evaluated within a simple Gamow like model. Figure 1 shows a model potential, from which the charged particle is emitted, in the form of a square well of radius R taking into account, on the outer side, the Coulomb potential V_C and (if necessary) the centrifugal potential V_l.

In this model the light charged particle has to penetrate the barrier from inside the nucleus at R up to the exit point at $\mathrm{R_{out}}$, where the kinetic energy of the particle is equal to the sum of Coulomb and centrifugal potential. The

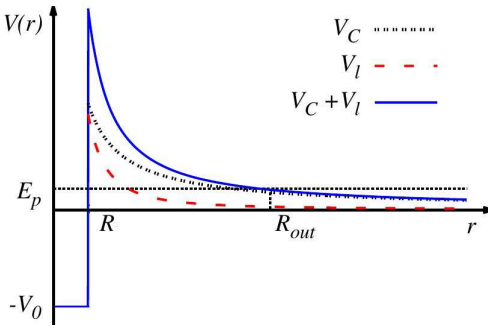

Figure 1. A charged particle of energy E_p penetrates a barrier (solid blue line) consisting of a square well, a Coulomb V_C (dotted line) and a rotational potential V_l (red dashed line), at radius R and leaving at radius $R_{\rm out}$.

half-life of the nucleus is then given by:

$$T_{1/2} = \frac{\ln 2}{\lambda}\, 10^h\,, \tag{1}$$

where h is the hindrance factor for odd-even (o-e) or odd-odd (o-o) nuclei ($h = 0$ for even-even (e-e) systems) and $\lambda = \nu P$, with ν the number of assaults per unit time against the barrier. Within the WKB approach, the probability P for barrier penetration is equal to

$$P = \exp\left[-\frac{2}{\hbar}\int_R^{R_{\rm out}} \sqrt{2\mu\,[V(r) - E_p]}\, dr\right]. \tag{2}$$

Here μ is the reduced mass, $V(r)$ the nuclear potential energy and $E_p = E_{\rm k}$ the kinetic energy of the emitted particle. R is the radial distance at the entrance point of the barrier and $R_{\rm out}$ the exit radius. In the case of α or cluster emission the centrifugal barrier V_l is simply absent as one can deduce from the experimental data.

2.1 Alpha particle emission

In the case of the emission of an α particle or a cluster, the probability of tunnelling through the barrier is given by:

$$P = \exp\left\{-\frac{2}{\hbar}\sqrt{2\mu Z_1 Z_2 e^2 R_{\rm out}}\left[\arccos\sqrt{\frac{R}{R_{\rm out}}} - \sqrt{\frac{R}{R_{\rm out}} - \left(\frac{R}{R_{\rm out}}\right)^2}\right]\right\}. \tag{3}$$

Here $R = r_0(A_1^{1/3} + A_2^{1/3})$ is the sum of the radii of the fragments of proton numbers Z_1 and Z_2 and mass numbers A_1 and A_2 (for α particles $Z_1 = 2$

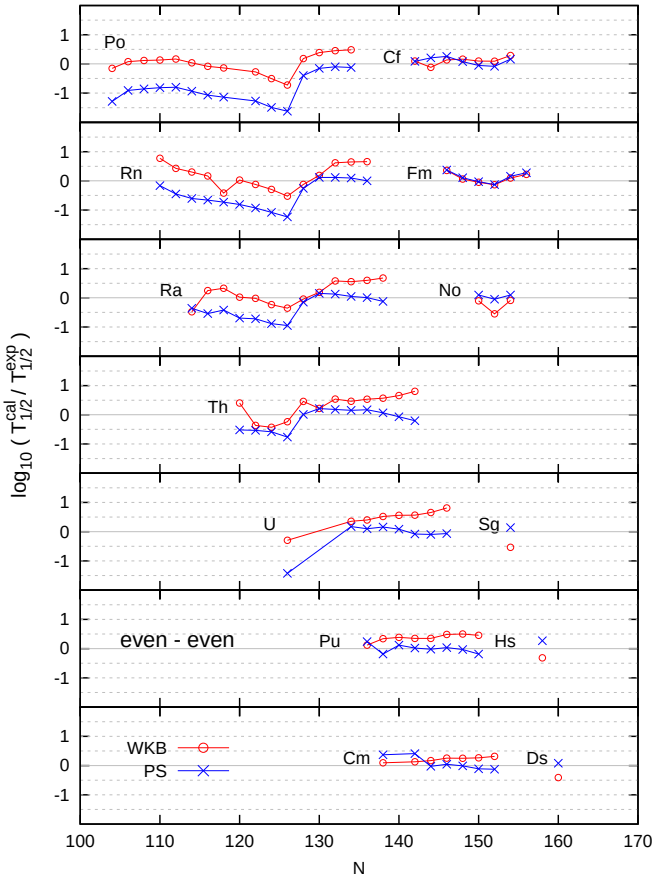

Figure 2. Deviations of the α emission half-lives (on a logarithmic scale) from the experimental data for even-even nuclei in different isotopic chains, evaluated in the 1-parameter WKB approach [2] (red circles) and the 4-parameter PS model (blue crosses) [3]. Taken from Ref. [2].

and $A_1 = 4$, $Z_2 = A - 2$ and $A_2 = A - 4$). In the ground state of a square well potential the number of assaults against the barrier is given by $\nu = \dfrac{\pi\hbar}{2\mu R^2}$, with $r_0 = 1.21$ fm [2]. Figure 2 shows the deviations of α emission half-lives $\log_{10}(T_{12}^{\rm cal})$ from the experimental data for even-even nuclei in the case of the 4-parameters PS approach of Ref. [3], and our 1-parameter WKB model [2], where this parameter is simply the radius constant r_0. One immediately concludes that the 1-parameter approach of Ref. [2] yields a much better description.

For the description of the decay of o-e, e-o or o-o nuclei another adjustable parameter is introduced, identical for each odd particle, namely the hindrance factor h that appears in Eq. (1).

2.2 Cluster radioactivity

Half-lives for cluster decay evaluated in our WKB approach [2] are presented in Figure 3 for even-even and odd A nuclei. Again a good reproduction of the experimental data is observed. When comparing the results obtained in our WKB approach with those of other models, like e.g. the one of Ren et al. [4], it turns out that our approach, relying on a single parameter for e-e nuclei yields better results (smaller r.m.s. deviation from the experiment) than other models that depend on several parameters.

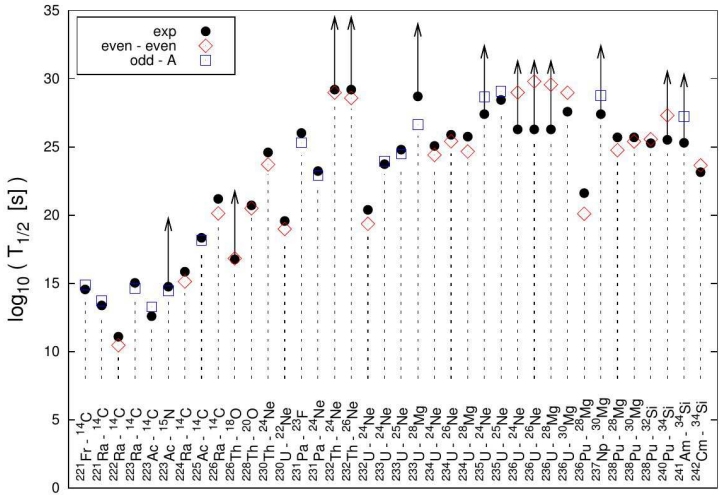

Figure 3. Comparison with the experimetal data of half-lives for cluster radioactivity obtained in our WKB approach [2] for even-even (red diamonds) and odd A (blue open squares) nuclei. Figure taken from Ref. [2].

2.3 Proton emission

In the case of proton emission Eq. (2) should be used with the following potential:

$$V(r) = \begin{cases} -V_0, & 0 \le r \le R\,, \\ \dfrac{(Z-1)e^2}{r} + \dfrac{\hbar^2 l(l+1)}{2\mu r^2}, & r > R\,, \end{cases} \tag{4}$$

where V_0 is the depth of the square well of radius $R = r_0[1+(A-1)^{1/3}]$ and the single adjustable parameter $r_0 = 1.21$ fm is exactly the same as the one which reproduces the life-times of α and cluster decays. Outside the barrier, only the Coulomb and the rotational potential are present. In addition we assume that the number of assaults against the barrier from the inside is given by the harmonic oscillator frequency of the Nilsson potential $\hbar\omega = 41/A^{1/3}$ MeV. Our results

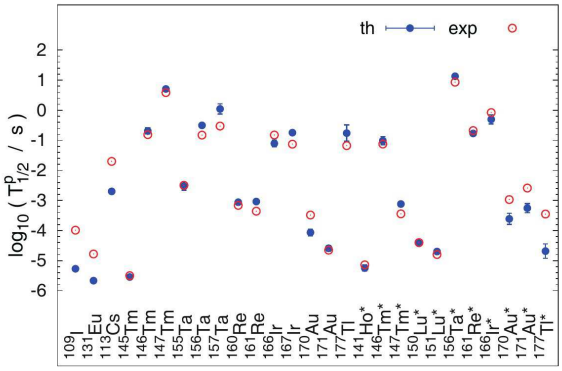

Figure 4. Comparison of proton-emission half-lives (on a logarithmic scale) obtained in the WKB approach (full blue circles) with the experimental data (open red circles). From [6].

for proton emission half-lives [5] shown in Figure 4 are again found to be very close to the experiment. The error bars that appear on some of the theoretical data are caused by the fact that the energy of the emitted particle for which the fit was carried out is measured with a certain uncertainty.

In Figure 5 the logarithm of the proton emission half-lives obtained in different models are displayed relative to the experimental data. Again, our WKB approach [5] relying on a single adjustable parameter for e-e, two for e-o, o-e, or o-o nuclei yield the best predictions.

The r.m.s. value obtained using our approach is comparable with the one of the 4-parameter Viola-Seaborg (V-S) type model of Ref. [7].

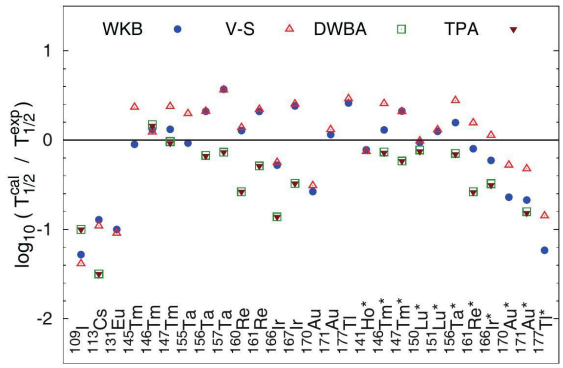

Figure 5. Calculated proton-emission half-lives, relative to the experimental data, obtained in different models with r.m.s. deviation from the experiment: WKB [6] r.m.s. = 0.36, V-S [7] r.m.s. = 0.37, DWBA [8] r.m.s. = 0.37, TPA [9] r.m.s. = 0.37. From [6].

3 Spontaneous Fission Probability

A proper description of spontaneous fission of nuclei requires the precise knowledge of the dependence of their potential energy on deformation. Swiatecki's topographical theorem [10] tells us that the macroscopic and the experimental masses at saddle point deformation are almost equal: $M^{\rm exp}_{\rm sadd} \approx M^{\rm mac}_{\rm sadd}$, which means that for the calculation of fission-barrier heights, only the macroscopic energy at the saddle point is needed.

One finds that the barrier heights obtained using Swiatecki's topographical theorem [11] with the LSD model [12] are, indeed, very close to the data as shown in Figure 6.

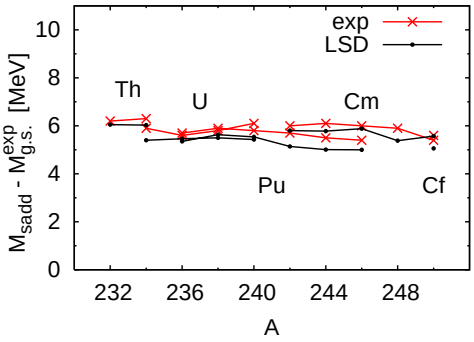

Figure 6. Fission barrier heights obtained using Swiatecki's topographical theorem [11] with the LSD model [12] compared to the experiment. Figure taken from Ref. [13].

Let us introduce a new coordinate x related to the fission path described by the length s of that path in the multidimensional deformation space

$$x(s) = \int_{s_0}^{s} \sqrt{\frac{B_{ss}(s')}{m}}\, ds' \ . \tag{5}$$

The coordinate x corresponds to the constant mass parameter m. This relation is obtained assuming that the kinetic energy operator in the x space is equal to the one in the s coordinate. The quantity B_{ss} that appears in Eq. (5) is the mass parameter in the s coordinate.

The potential $V[s(x)]$ in the new coordinate x that has to be overcome is approximated by two inverted parabolas as visualized in Figure 7. Choosing the maximum $V_{\rm sadd}$ of the potential as the cusp of the parabolas, the two-parabola approximation $\widetilde{V}(x)$ of that potential can be written as

$$\widetilde{V}(x) = \begin{cases} V_{\rm sadd} - \frac{1}{2}\, C_l\, x^2 & \text{for } x \ < \ 0 \ , \\ V_{\rm sadd} - \frac{1}{2}\, C_r\, x^2 & \text{for } x \ > \ 0 \ , \end{cases} \tag{6}$$

where C_l and C_r are the respective stiffness of left and right parabolas.

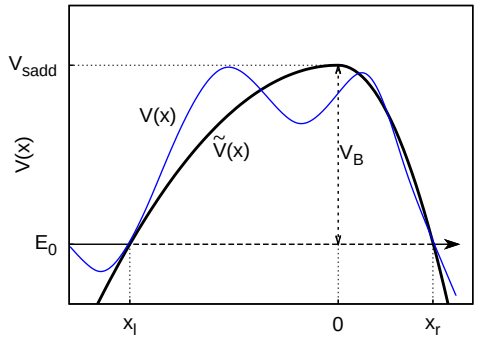

Figure 7. Two-parabola approximation $\widetilde{V}(x)$ of a fission barrier $V(x)$, with $V_{\rm B}$ the barrier height above the particle energy E_0, $V_{\rm sadd}$ the saddle point energy, and x_l and x_r the entrance and exit points of the barrier. From Ref. [5].

3.1 Fission-barrier penetration in the WKB approximation

The spontaneous fission half–life is given by:

$$T_{1/2}^{\rm sf} = \frac{\ln 2}{\nu P}\,, \qquad \text{where} \qquad P = \frac{1}{1+\exp\{2S(L)\}} \tag{7}$$

is the probability for penetrating the barrier and ν the frequency of assaults against the fission barrier. The WKB action-integral along the fission path $L(s)$ reads:

$$S(L) = \int_{s_l}^{s_r} \sqrt{\frac{2}{\hbar^2}\,B_{ss}[V(s)-E_0]}ds \approx \int_{x_l}^{x_r} \sqrt{\frac{2m}{\hbar^2}[\widetilde{V}(x)-E_0]}\,dx\,. \tag{8}$$

Using the inverted-parabola approximation of Figure 7 the action integral becomes

$$S = \frac{\pi}{2\hbar}V_B\left(\sqrt{\frac{m}{C_l}}+\sqrt{\frac{m}{C_r}}\right) = \frac{\pi}{\hbar}V_B\,\frac{\omega_l+\omega_r}{2\,\omega_l\,\omega_r} \equiv \frac{\pi}{\hbar}V_B\,\tilde{\omega}^{-1}\,, \tag{9}$$

where V_B is the barrier height, $\omega_l = \sqrt{C_l/m}$ and $\omega_r = \sqrt{C_r/m}$ are the inverted harmonic oscillator frequencies of left and right parabolas and $\tilde{\omega}$ their average.

For $S > 1$ the logarithm of the spontaneous fission half-life, expressed in time units, takes the form:

$$\log_{10}(T_{1/2}^{\rm sf}) = \frac{2\pi}{\hbar\tilde{\omega}}V_B - \log[\nu\ln 2] \approx \frac{2\pi}{\hbar\tilde{\omega}}(M_{\rm sadd}^{\rm LSD} - M_{\rm exp}) - \log[\nu\ln 2] \tag{10}$$

which can be written as follows (see also Ref. [14])

$$\log_{10}(T_{1/2}^{\rm sf}) + \frac{2\pi}{\hbar\tilde{\omega}}\delta M = \frac{2\pi}{\hbar\tilde{\omega}}\,V_B^{\rm LSD} - \log_{10}[\nu\ln 2] \tag{11}$$

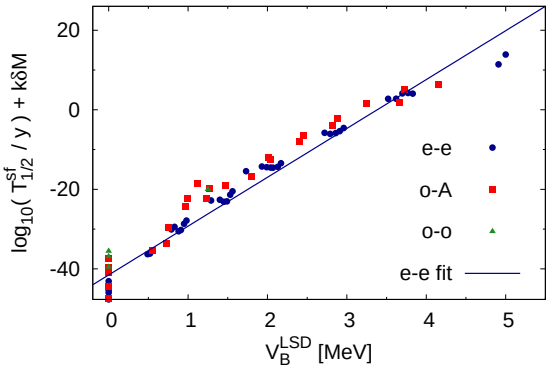

Figure 8. Experimental spontaneous fission half-lives for even-even (e-e), odd-odd (o-o) and odd mass (o-A) nuclei, corrected by the microscopic ground-state energy as function of the macroscopic LSD barrier height. The solid line represents the average trend for e-e isotopes. The adjustable parameter k is chosen as $k = 7.7$ MeV^{-1}. From Ref. [5].

where $\delta M = M_{\rm exp} - M_{\rm sph}^{\rm LSD}$ is the microscopic ground-state correction energy and $V_B^{\rm LSD} = M_{\rm sadd}^{\rm LSD} - M_{\rm sph}^{\rm LSD}$ the macroscopic barrier height.

The experimental spontaneous fission half-lives are displayed in Figure 8 for different nuclei as function of the LSD [12] fission barriers heights and compared to the fit presented above. Knowing the average trend and the ground-state mass correction one can easily obtain an estimate of the fission live-times. The results for even-even nuclei are displayed in Figure 9. A very nice agreement with the experimental data is observed. For odd-odd and odd-A nuclei it is comparable, when introducing a hindrance factor $h = 2.5$ for each odd particle. Experimental microscopic corrections have been used where available. Otherwise these were taken from Möller's mass table [15].

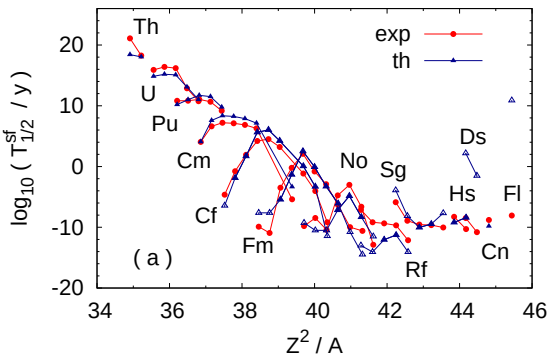

Figure 9. Spontaneous fission half-lives of even-even isotopes obtained in our model [5, 14] for different isotopic chains as compared to the experiment. From Ref. [5].

4 Shape Parametrisations of Nuclei

A proper low-dimensional description of nuclear shapes, in particular of fissioning nuclei, is one of the most difficult task nuclear physicists have been confronted with since the first paper of Bohr and Wheeler [16] on the theory of nuclear fission.

Among the most popular shape parametrisations one finds:

- the classical expansion of the nuclear surface in spherical harmonics proposed by Lord Rayleigh in 19th century,
- the so-called Quadratic Surfaces of Revolutions by J.R. Nix [17] in 1969, extensively used by P. Möller [18],
- the Cassini ovaloids of Pashkevich [19] from 1971,
- the so-called Funny-Hills (FH) parametrisation introduced by Brack et al. [20] of 1972, and its modification (MFH - Gauss neck and nonaxiality) [21] from 2004,
- the expansion in a series of Lagrange polynomial by Trentalange, Koonin and Sierk [22] from 1980,
- the Fourier expansion in trigonometrical functions by Pomorski et al. [23] from 2015.

Among all these shape parametrisations the one by Lord Rayleigh is probably the most popular and widely used one. For the correct description of fission barrier heights in the actinide region it requires, however, at least 12 coefficients, whereas only 3 are necessary in the Fourier expansion of Ref. [23].

4.1 Fourier expansion of nuclear shapes

The surface of a nucleus can be expressed in cylindrical coordinates $\{\rho_s, \varphi, z\}$, where ρ_s denotes the distance of a surface point from the symmetry axis. A typical fission shape is shown in Figure 10.

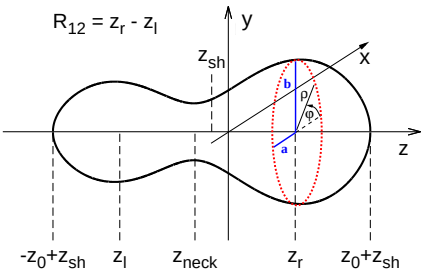

Figure 10. Triaxial nuclear shape in cylindrical coordinates

Triaxial shapes can be described by introducing a nonaxiality parameter

$$\eta = \frac{b-a}{a+b}\,,$$

where a and b are the half-axes of the spheroid with $\rho_s^2(z) = a(z)b(z)$. In the axially symmetric case the distance from the nuclear surface is:

$$\frac{\rho_s^2(z)}{R_0^2} = \sum_{n=1}^{\infty} \left[a_{2n} \cos\left(\frac{(2n-1)\pi}{2} \frac{z - z_{sh}}{z_0} \right) + a_{2n+1} \sin\left(\frac{2n\pi}{2} \frac{z - z_{sh}}{z_0} \right) \right] , \tag{12}$$

where R_0 is the radius of the corresponding spherical shape, while $2z_0$ represents the elongation of the nucleus along the symmetry z axis. In order to describe non-axial shapes, the profile function is written as

$$\varrho_s^2(z, \varphi) = \rho_s^2(z) \frac{1 - \eta^2}{1 + \eta^2 + 2\eta \cos(2\varphi)} . \tag{13}$$

The convergence of the above defined Fourier expansion is extremely rapid as becomes obvious from Figure 11 that shows the LSD fission barrier of ^{232}Th as function of the distance R_{12} between the two fragments obtained by different truncations.

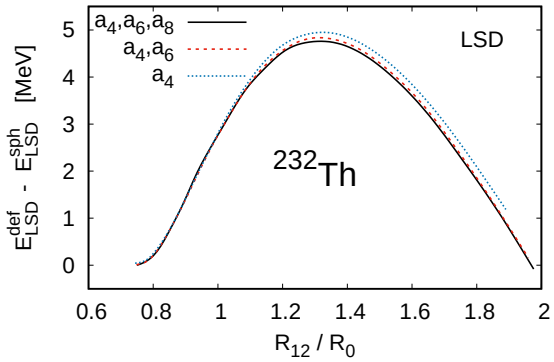

Figure 11. LSD deformation energy for ^{232}Th obtained with the inclusion of the indicated a_{2n} coefficients of the Fourier expansion. Figure taken from Ref. [24].

As one concludes from the figure, the height and shape of the liquid-drop type barrier is already almost perfectly described with only two parameters. Notice that in such a left-right symmetric case only even multipolarities contribute. The volume conservation condition leads to the following relation:

$$\frac{\pi}{3c} = \sum_{n=1}^{\infty} (-1)^{n-1} \frac{a_{2n}}{2n-1} , \tag{14}$$

where $c = z_0/R_0$ is the (Funny-Hills) elongation parameter.

In presence of the odd-deformations one introduces a shift parameter

$$z_{sh} = \frac{3c^2}{2\pi} R_0 \sum_n (-1)^n \frac{a_{2n+1}}{n} \tag{15}$$

in the definition of ρ_s^2 such that the centre of mass of the shape is always located at the origin. For symmetric fission the scission point is always located at $z = 0$ which implies: $\sum_{n=1}^{\infty} a_{2n} = 0$. For odd-deformations the neck appears approximately at:

$$z_{\rm neck} = z_{sh} + z_0\, t\frac{4}{\pi}\,\frac{\sum\limits_n n\, a_{2n+1}}{\sum\limits_n (2n-1)^2\, a_{2n}}\ , \tag{16}$$

which has to be taken into account when evaluating the relative distance R_{12} between the mass centres of the two nascent fragments.

5 Potential Energy Surfaces

In the liquid drop (LD) model the potential energy of a deformed nucleus is given by

$$\frac{\Delta E({\rm def})}{E_{\rm surf}({\rm sph})} = [B_{\rm surf}({\rm def}) - 1] + 2\chi[B_{\rm Coul}({\rm def}) - 1]\ , \tag{17}$$

where $\Delta E({\rm def}) = E_{\rm LD}({\rm def}) - E_{\rm LD}({\rm sph})$ is the difference between the liquid-drop energies of deformed and spherical nucleus and $B_{\rm surf}$ and $B_{\rm Coul}$ are the ratios of surface and Coulomb energy of the deformed relative to the spherical shape. By

$$\chi = \frac{E_{\rm Coul}({\rm sph})}{2E_{\rm surf}({\rm sph})}\ , \tag{18}$$

one introduces the so-called fissility parameter.

Figure 12 shows the deformation energy of a system with $\chi = 0.8$ as function of a_2 and a_4. What we dislike about this presentation is : 1) we would like to keep the hexadecapole type parameter q_4 as small as ever possible; 2) we would

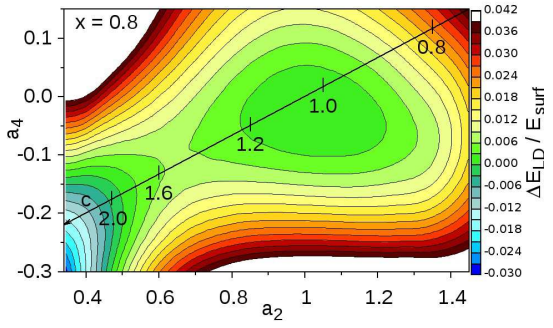

Figure 12. LSD deformation energy for a system with fissility χ=0.8, normalized to the surface energy E_{surf}, in the (a_2, a_4) plane. Figure taken from Ref. [24].

like the quadrupole parameter q_2 to increase with increasing elongation, which is not the case with the present definition. To satisfy these two requests and, at the same time, keep higher-order parameters as small as possible, we introduce the following new coordinates:

$$q_2 = \frac{a_2^{(0)}}{a_2} - \frac{a_2}{a_2^{(0)}}\,, \qquad q_3 = a_3\,, \qquad q_4 = a_4 + \sqrt{(\frac{q_2}{9})^2 + (a_4^{(0)})^2}\,,$$
$$q_5 = a_5 - (q_2 - 2)\,\frac{a_3}{10}\,, \qquad q_6 = a_6 - \sqrt{(\frac{q_2}{100})^2 + (a_6^{(0)})^2}\,, \tag{19}$$

where q_2 describes the elongation of the shape, q_3 its left-right asymmetry, and q_4 the neck formation. The Fourier expansion coefficients of a sphere are given by $a_2^{(0)} = 1.03205$, $a_4^{(0)} = -0.03822$, and $a_6^{(0)} = 0.00826$.

A few examples of the LSD potential energy surfaces in the (q_2, q_4), (q_2, q_3), (q_2, q_6) and (q_2, q_5) planes are presented in Figure 13.

When calculating the deformation energy of a nucleus, the microscopic (shell and pairing) corrections must be included in addition to the liquid-drop energy. These microscopic corrections are determined here by the Strutinsky [25] method together with a monopole BCS pairing force. Figure 14 shows the total deformation energy relative to the spherical LSD energy in the (q_2, q_3) plane for the nucleus ^{236}Pu. Two prolate minima can be seen at $q_2 \approx 0.35$ and $q_2 \approx 0.75$.

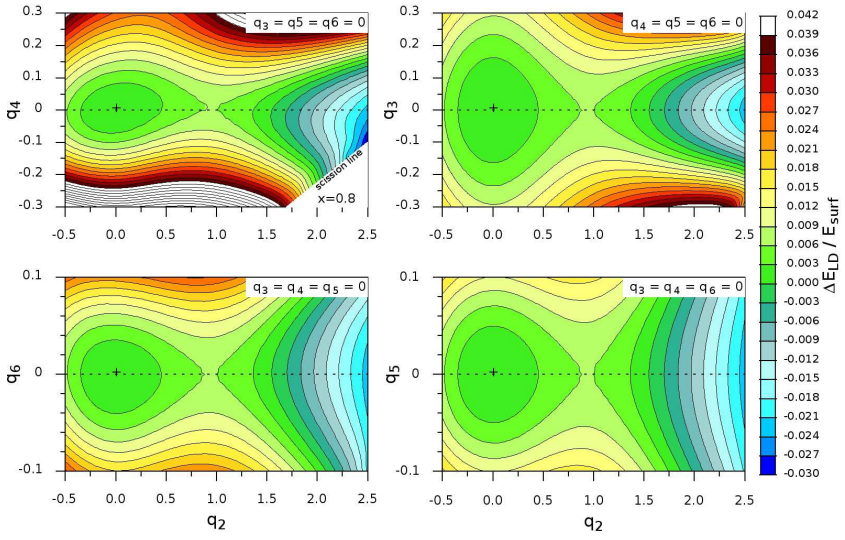

Figure 13. Same as Figure 12 but in the (q_2, q_4), (q_2, q_3), (q_2, q_6) and (q_2, q_5) planes. Figure taken from Ref. [24].

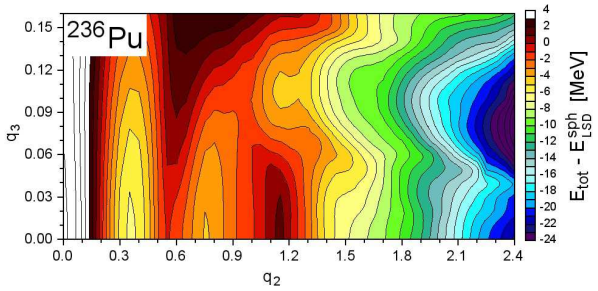

Figure 14. Total potential energy surface, relative to the spherical LSD energy, as function of the elongation and asymmetry parameters q_2 and q_3 for ^{236}Pu.

The total-energy cross-section for ^{236}Pu, again relative to the LSD value for the sphere, is presented in Figure 15 in the (q_3, q_4) plane at a large elongation (close to the scission point) $q_2 = 2.25$.

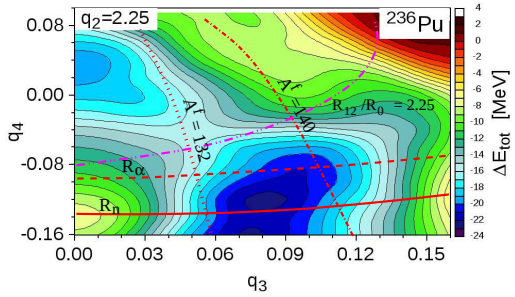

Figure 15. Same as Figure 14 but now as function of q_3 and the neck parameter q_4 for an elongation of $q_2 = 2.25$. The distance R_{12} of the nascent fragments given by $2.25R_0$ is represented by the dash-double-dotted line. Dotted and dash-dotted lines show the deformation where the mass of the heavy fragment is equal to 132 and 140 respectively, while solid and dashed lines indicate where the neck is respectively of the size of a nucleon or an α-particle.

The lines labelled A_f define the location in the deformation energy where the heavy fragment is of the size of the indicated mass ($A = 132$ and $A = 140$ respectively), whereas the lines labelled R_n and R_α indicate where the neck is of the size of a nucleon and an α-particle respectively. It is clear that somewhere in that region the transition form a mono-nuclear to a di-nuclear system will take place.

The potential energy surfaces (PES) evaluated in our model were used in [27] to obtain a rough estimate of the fission-fragment mass yield for the Pu isotopic chain ($^{236-246}$Pu). The probability-density distribution of a nucleus evolving from the exit point of the barrier down to the scission configuration on the (q_2, q_3, q_4) plane was estimated using the Born-Oppenheimer approximation.

A WKB type wave function was used to describe the motion towards fission (q_2) while the perpendicular (or better to say quasi-perpendicular) modes on the $(q_3, q_4; q_2)$ plane were described by a normalized Wigner function proportional to $\exp\{-[V(q_3, q_4; q_2) - V(q_3^{\rm eq}, q_4^{\rm eq}; q_2]/E_0\}$. We have tested several neck-rupture probability functions and found that the final result for the fission-fragment mass distribution is quite insensitive to that choice. We have therefore used a Gauss function of the form $\exp[-\ln 2(r_{\rm neck}/d)^2]$ that depends on the neck size $r_{\rm neck}$ [27]. The results of such fission fragment mass yields are shown for the Pu isotopic chain in Figure 16, where the only two free parameters, the energy $E_0 = 1$ MeV in the Wigner function and the width parameter $d/R_0 = 0.15$ in the neck-breaking probability were adjusted to the mass yield

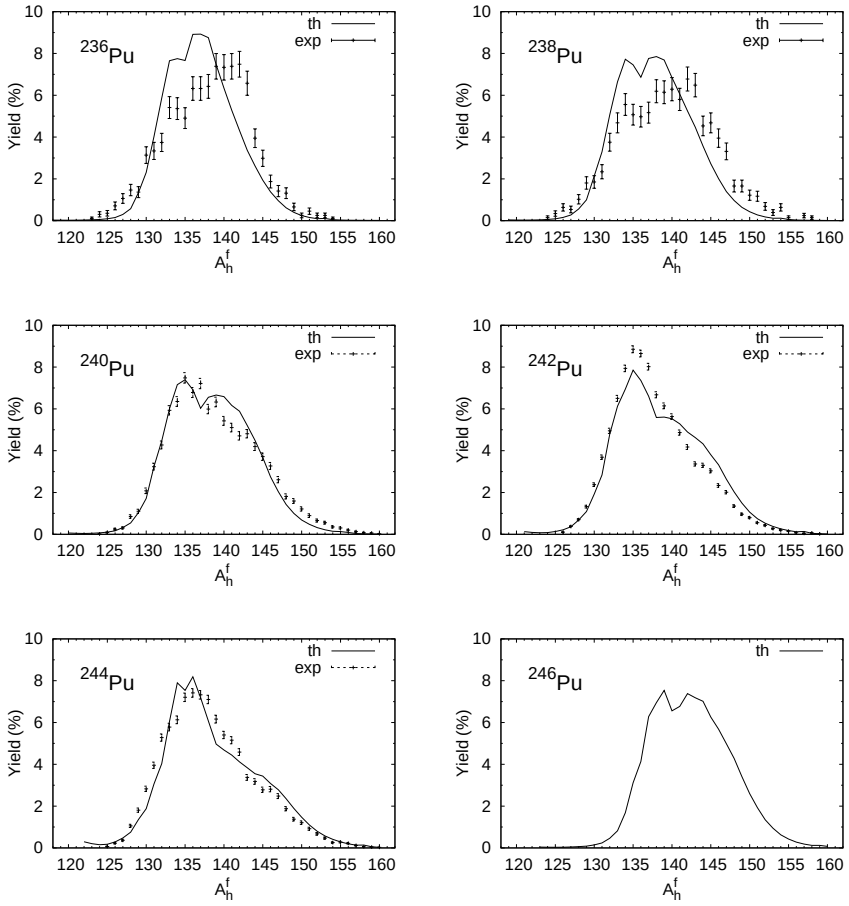

Figure 16. Fission fragment mass yields of $^{236-246}$Pu as compared to the experimental data taken from [26].

of ^{240}Pu. Keeping in mind that no dynamical effects have been taken into account in our approach, one could consider the reproduction of the experimental data [26] as rather satisfactory. It was shown in addition in Ref. [27] that the total kinetic energy distribution of the fission fragments is also reproduced fairly well which proves that the shapes (and consequently the Coulomb energy) of the nascent fragments are well described by our 3D parametrisation.

6 Conclusions

We have presented a simple WKB model with only 1 adjustable parameter (for even-even systems, 2 for odd A and odd-odd nuclei) to evaluate the probabilities for emission of a proton, alpha and cluster nucleus. Ground-state shell and pairing effects determine the fission-barrier heights. It was shown that the role of the microscopic effects at the saddle point is, however, almost negligible. Spontaneous fission life-times are mostly determined by the microscopic energy correction in the ground-state and the macroscopic fission barrier. A new Fourier expansion of nuclear shapes turns out to represent a extremely effective way of describing the shapes of fissioning nuclei with a minimal number of deformation parameters. It was also shown that a three dimensional quantum mechanical model that couples elongation, neck and mass asymmetry modes is able to describe the main features of the fragment mass yields.

Acknowledgements

This work has been partly supported by the Polish-French COPIN-IN2P3 collaboration agreement under project number 08-131 and by the Polish National Science Centre, grant No. 2013/11/B/ST2/04087.

References

[1] G. Gamow, *Z. Phys.* **51** (1928) 204.
[2] A. Zdeb, M. Warda, and K. Pomorski, *Phys. Rev. C* **87** (2013) 024308.
[3] A. Parkhomenko and A. Sobiczewski, *Acta Phys. Polon. B* **36** (2005) 3095.
[4] Z. Ren, C. Xu, and Z. Wang, *Phys. Rev. C* **70** (2004) 034304.
[5] K. Pomorski, M. Warda and A. Zdeb, *Phys. Scr.* **90** (2015) 114013.
[6] A. Zdeb, M. Warda, C.M. Petrache, and K. Pomorski, *Eur. Phys. J. A* **52** (2016) 323.
[7] J.M. Dong, H.F. Zhang, G. Royer, *Phys. Rev. C* **79** (2009) 054330.
[8] H. Feshbach, "*Theoretical Nuclear Physics: Nuclear Reactions*" (Wiley, New York, 1992).
[9] S.A. Gurvitz, *Phys. Rev. A* **38** (1988) 1747.
[10] W.D. Myers, W.J. Świątecki, *Nucl. Phys. A* **612** (1997) 249.
[11] W.D. Myers, W.J. Świątecki, *Nucl. Phys. A* **601** (1996) 141.
[12] K. Pomorski and J. Dudek, *Phys. Rev. C* **67** (2003) 044316.

[13] A. Dobrowolski, B. Nerlo-Pomorska, K. Pomorski, *Acta Phys. Pol. B* **40** (2009) 705.
[14] W.J. Świątecki, *Phys. Rev.* **100** (1955) 937.
[15] P. Möller, J.R. Nix, W.D. Myers, W.J. Świątecki, *At. Data Nucl. Data Tab.* **59** (1995) 185.
[16] N. Bohr, J.A. Wheeler, *Phys. Rev*. **56** (1939) 133.
[17] J.R. Nix, *Nucl. Phys. A* **130** (1969) 241.
[18] P. Möller, D.G. Mainland, A. Sierk, and A. Ivamoto, *Nature A* **409** (2001) 785.
[19] V.V. Pashkievich, *Nucl. Phys. A* **169** (1971) 275.
[20] M. Brack et al., *Rev. Mod. Phys.* **44** (1972) 320.
[21] J. Bartel, A. Dobrowolski, and K. Pomorski, *IJMP E* **16** (2007) 459.
[22] S. Trentalange, S.E. Koonin and A.J. Sierk, *Phys. Rev. C* **22** (1980) 1159.
[23] K. Pomorski, B. Nerlo-Pomorska, J. Bartel, and C. Schmitt, *Acta Phys. Pol. Supl. B* **8** (2015) 667.
[24] C. Schmitt, K. Pomorski, B. Nerlo-Pomorska, and J. Bartel, *Phys. Rev. C* **95** (2017) 034612.
[25] V.M. Strutinsky, *Nucl. Phys. A* **95** (1969) 420.
[26] L. Démattè et al., *Nucl. Phys. A* **617** (1997) 331.
[27] K. Pomorski, B. Nerlo-Pomorska, J. Bartel, and C. Schmitt, submitted for publication in *EPJ Conf. Series*.